LSCF-CGO nanocomposite cathodes deposited in a single step by spray-pyrolysis

L. dos Santos-Gómez[a], J.M. Porras-Vázquez[a], E.R. Losilla[a], F. Martín[b], J.R. Ramos-Barrado[b], D. Marrero-López[b,*]

[a]*Universidad de Málaga, Departamento de Química Inorgánica, Cristalografía y Mineralogía, 29071-Málaga, Spain.*

[b] *Universidad de Málaga, Departamento de Física Aplicada I, Laboratorio de Materiales y Superficie, 29071-Málaga, Spain.*

ABSTRACT

$La_{0.6}Sr_{0.4}Co_{0.2}Fe_{0.8}O_{3-\delta}$-$Ce_{0.9}Gd_{0.1}O_{1.95}$ (LSCF-CGO) nanostructured cathodes with different LSCF-content are prepared in a single step by spray-pyrolysis deposition, simplifying notably the fabrication process compared to the traditional methods. The phase formation, structure, microstructure and electrochemical properties of the cathodes are investigated as a function of the CGO-content and the temperature by using X-ray diffraction, electron microscopy and impedance spectroscopy. The addition of CGO to LSCF limits the grain growth, giving rise to fine particles of approximately 30 nm of diameter after sintering at 800 ºC. A small particle size of 50 nm is retained even after sintering at 1000 ºC. However, the polarization resistance, determined by impedance spectroscopy, is not significantly improved with the CGO-addition. The performance of these nanocomposite electrodes, investigated in NiO-CGO anode-supported cells, shows an improved power density of 0.9 Wcm^{-2} at 650 ºC, compared to 0.56 Wcm^{-2} for a conventional screen-printed cathode.

Keywords: Solid Oxide Fuel Cells, composite cathode, $La_{0.6}Sr_{0.4}Co_{0.2}Fe_{0.8}O_{3-\delta}$, $Ce_{0.9}Gd_{0.1}O_{1.95}$, spray-pyrolysis.

* Corresponding author.

E-mail address: marrero@uma.es (David Marrero-López)

Present address: Dpto. de Física Aplicada I, Laboratorio de Materiales y Superficies, Facultad de Ciencias, Campus de Teatinos, Universidad de Málaga, 29071-Málaga, Spain.

Tel: +34 952137057, Fax: +34 952132382

1. Introduction

Solid Oxide Fuel Cells are efficient electrochemical devices for direct conversion of fuels to electrical energy with low pollutant emissions [1-3]. However, the commercialization of this technology is still hindered by the high operation temperatures, and the consequent premature performance degradation. For this reason, lowering the operation temperature to the range of 400-650 ºC would lead to significant advantages, including the use of less expensive fabrication materials and lower degradation rates [4].

Nevertheless, the performance at low operating temperature is limited by the slow kinetic of the cathode for the oxygen reduction. The most commonly used cathode is the strontium doped lanthanum manganite, $La_{0.8}Sr_{0.2}MnO_{3-\delta}$ (LSM), which has high electronic conductivity and acceptable activity for oxygen reduction reaction (ORR) at temperatures above 800 ºC [5]. However, LSM is a predominant electronic conductor with negligible ionic conductivity, and therefore, the oxygen reduction reaction is mainly limited at the three phase boundary (TPB) near the electrolyte/electrode interface. Thus, the development of efficient cathode materials with high catalytic activity for the ORR is one of the main goals to improve the performance at low operating temperature. In this regard, $La_{0.6}Sr_{0.4}Co_{0.2}Fe_{0.8}O_{3-\delta}$ (LSCF) exhibits improved mixed ionic-electronic conductivity, and therefore suitable for applications at low temperatures [6,7].

The use of nanostructured electrodes with greatly increased TPB sites for the ORR is an alternative approach to improve the cathode performance [8]. Different preparation methods have been used to obtain nanostructured LSCF cathodes, including nanoparticles from precursor routes, infiltration into a porous electrolyte scaffold and spray-pyrolysis deposition [9-14]. In particular, spray-pyrolysis is an attractive method for producing large-area electrodes, with a number of advantages, such as low cost and feasibility for industrial implementation. In this method a precursor solution is sprayed onto a heating substrate and films with different morphology, i.e. dense, porous, cracked and coral-type, are obtained by tailoring the deposition conditions [15-18]. These nanostructured electrodes exhibited polarization resistance as low as 0.1 Ωcm^2 at 600 ºC; one order of magnitude inferior to that reported for a traditional cathode deposited by screen-printing method.

The addition of a second phase with high mixed ionic electronic conductivity to LSCF, is another strategy to increase the TPB sites, and consequently, the performance. Typically, CGO and LSCF are combined due to the high compatibility between both materials. All the previous studies concluded that the LSCF-CGO cathodes exhibit lower polarization resistance [19-25]. The optimum CGO content in LSCF-CGO cathodes, corresponding to electrical percolation threshold, varies in the literature between the 40 and 60 wt.%.

The use of nanocomposites electrodes are expected to further improve the performance. However, the polarization resistance of LSCF-CGO, prepared by a single solution spray-pyrolysis, varies in broad range from 0.1 to 2 Ωcm^2 for 60 wt.% LSCF-CGO at 600 ºC [26-29]. These differences are explained by differences in the microstructure of the electrodes as well as the different electrolyte used, YSZ and CGO [26,27]. Moreover, to the best of our knowledge, there are not studies on the performance of these nanocomposite electrodes in real SOFC devices.

In this study, $La_{0.6}Sr_{0.4}Co_{0.2}Fe_{0.8}O_{3-\delta}$ - $Ce_{0.9}Gd_{0.1}O_{1.95}$ (LSCF-CGO) nanocomposite cathodes with different fractions of LSCF, between 50 and 100 wt.%, are prepared in a single step by a spray-pyrolysis deposition method and a precursor water solution containing all cations in stoichiometric amounts. The nanostructured materials have been deeply investigated by different structural, microstructural and electrical techniques, including X-ray diffraction; scanning and transmission electron microscopy; and impedance spectroscopy. Finally, for the first time, the performance of a nanocomposite cathode obtained from a single solution is investigated in anode supported SOFCs, and the results are compared with conventional electrodes deposited by screen-printing method.

2. Experimental

2.1. Materials preparation.

$La_{0.6}Sr_{0.4}Co_{0.8}Fe_{0.2}O_{3-\delta}$ - $Ce_{0.9}Gd_{0.1}O_{1.95}$ (LSCF-CGO) composite cathodes with different LSCF content (100, 70, 60 and 50 wt.%) were prepared by using a conventional spray-pyrolysis deposition method. The composition of the composite cathodes is hereafter denoted as *X*LSCF, where *X* represents the content of LSCF (wt.%).

The precursor solutions were obtained by dissolving stoichiometric quantities of $La(NO_3)_3 \cdot 6H_2O$, $Sr(NO_3)_2$, $Co(NO_3)_2 \cdot 6H_2O$, $Fe(NO_3)_3 \cdot 9H_2O$, $Ce(NO_3)_3 \cdot 6H_2O$ and $Gd(NO_3)_3 \cdot 6H_2O$ in distilled water. All of them supplied by Sigma-Aldrich and purity above 99%. The solutions with concentration 0.02 mol L^{-1} were pumped to the spray gun with a flow rate of 0.30 mL min^{-1} and atomized with air at a pressure of 2 atm. The substrates are previously heated onto an aluminium plate at 250 ºC. The temperature is monitored with a thermocouple placed just below the substrates. The substrates are continuously moved at a constant speed underneath the spray nozzle [30,31]. The deposition time and nozzle-substrate distance were 60 min and 25 cm, respectively. After the deposition, the electrodes were calcined in a furnace between 650 and 1000 ºC for 2 h in air atmosphere.

The electrodes were deposited on amorphous quartz plates for a more accurate structural analysis and on CGO electrolyte in symmetrical cells for the electrochemical characterization. The CGO pellets were prepared by pressing the commercial CGO powders (Rhodia) into discs of 10 and 1 mm of diameter and thickness, respectively, followed by sintering at 1400 ºC for 4 h.

2.2. Characterization.

Phase analysis was carried out by X-ray powder diffraction (XRD) with a PANalytical Empyrean equipped with $CuK\alpha_{1,2}$ radiation. The phase identification and structural analysis were performed with X'Pert HighScore Plus and the GSAS suite programs, respectively [32,33].

The morphology and composition of the electrodes were investigated by field emission scanning electron microscopy (FEI-SEM, Helios Nanolab 650) and high-angle annular dark-field scanning transmission electron microscopy (HAADF-STEM) (FEI, Talos F200X).

The electrode polarization resistance of the cathodes in symmetrical cell configuration was investigated by impedance spectroscopy with a Solartron 1260 Frequency Response Analyzer (FRA). Pt-ink and meshes were used as current collectors. The spectra were collected in the 0.01-10^6 Hz frequency range with an AC perturbation of 50 mV between 350 and 650 ºC in static air atmosphere. The data were fitted to equivalent circuits using the ZView software [34].

Anode supported half cells, NiO(60wt.%)-CGO/CGO, were fabricated following the procedure described elsewhere [35]. The 60LSCF composite cathode was deposited by spray-pyrolysis through a circular shadow mask of 0.3 cm^2 placed onto the electrolyte layer. The single cell was sealed on an alumina tube support with a ceramic paste (Ceramabond 668, Aremco). The current–voltage and impedance plots of the single cells were collected using a Bio-Logic VSP potentiostat/galvanostat/FRA at operating temperatures between 450 and 650 ºC. Static air and humidified H_2 (3 vol.% water) were used as the oxidant and fuel gases, respectively. For the sake of comparison, a similar cell with a traditional cathode was prepared and tested under identical conditions. For this purpose, 60 wt.% CGO and 40 wt.% LSCF powders, obtained from freeze-drying precursors, were mixed in a planetary ball milling with Decoflux as binder material. The resulting ink was screen-printed onto the electrolyte and sintered at 1000 ºC for 1 h [18].

3. Results and Discussion

3.1. Phase composition

Fig. 1 shows representative XRD patterns for the blank cathode (100LSCF) and a nanocomposite cathode with 50 wt.% of LSCF (50LSCF) deposited by spray-pyrolysis at 250 ºC on quartz plates. All the as-prepared samples are amorphous at 250 ºC. 100LSCF crystallizes with rhombohedral perovskite structure at 650 ºC without the presence of secondary phases (Fig. 1a). In the case of the 50LSCF, broad diffraction peaks are observed after calcining at 650 ºC, and it is not possible to distinguish between the CGO and LSCF reflections (Fig. 1b). The increase of temperature at 800 ºC improves the crystallinity and two different crystalline phases with perovskite and fluorite-type structures are clearly discernible. The position of the peaks matches well with the theoretical patterns of LSCF and CGO (ICSD 187793 and 1848585) [36].

The XRD patterns of cathodes with different CGO-content and deposited on CGO pellets are given as supplementary content in Fig. S1. For all compositions, LSCF and CGO phases are formed at 800 ºC without secondary phases. The main difference between the patterns is the relative intensity of LSCF and CGO reflections, which varies depending on the LSCF-content. Note that unlike Figure 1, the narrower diffraction peaks of the CGO substrate overlap with those of the composite electrode, which results in an inaccurate phase quantification by Rietveld method. For this reason, the phase quantification is only presented for those samples prepared on amorphous quartz substrates.

The XRD patterns were analyzed by the Rietveld method in the space groups $Fm\bar{3}m$ for CGO and $R\bar{3}c$ for LSCF (supplementary content Fig. S2) [33]. In the case of the composite cathodes, deposited on CGO pellets, a second fluorite phase associated with the substrate was considered for the fitting. During the Rietveld analysis, the following parameters were refined: scale factors, background, zero shift, pseudo-Voigt,

asymmetry for the peak-shape and preferential orientation. The occupation factors for the cation sites were fixed and not refined. Fig S2 shows some examples of the Rietveld fitting for 50LSCF deposited onto quartz and CGO substrates; and the resulting structural parameters are listed in Table S1. The agreement factors are rather good, R_F varies between 3.2 and 5.4%. In addition, the phase quantification, estimated by the Rietveld refinement, is in accordance with the nominal one. Regarding the unit cell volume of LSCF and CGO, these vary slightly for the different compositions and substrates. The volume of LSCF varies between 352.09(4) and 352.58 $Å^3$, while the CGO volume takes values in the range of 159.11(1)-159.32(2) $Å^3$, which is similar to that of the CGO substrate, about 159.25(2)-159.32(4) $Å^3$. These results seem to indicate that LSCF and CGO electrodes have similar cation stoichiometry, independently of the CGO-content. Nevertheless, the incorporation of minor amounts of Fe, Co and La into the CeO_2 lattice is not ruled out as observed in previous studies [37]. It has to be also mentioned that minor cation interdiffusion between LSCF and CGO has not detrimental effects on the electrical conductivity or electrocatalytic activity for oxygen reduction. For example, Co incorporation into the CGO lattice increases the electronic conductivity, which is beneficial for the performance of the composite cathode [37].

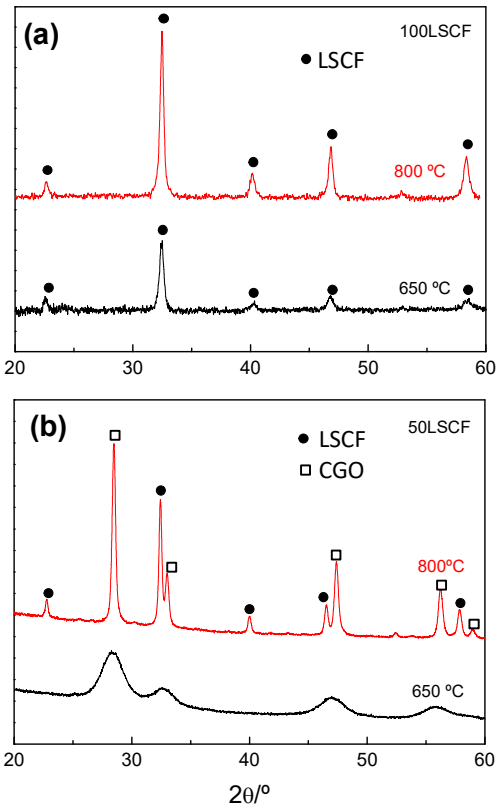

Fig. 1. XRD patterns of (a) 100LSCF and (b) 50LSCF cathodes deposited by spray-pyrolysis onto quartz substrates and calcined at 650 and 800 ºC for 2 h.

3.2. Microstructure

The morphology of the cross-section of the cathodes was examined by SEM (Fig. 2). The thickness of the cathodes is about 6 μm and they exhibit large porous due to the removal of residual solvents during the post-thermal treatment at high temperature (Fig. 2a). The porosity, about 50%, was estimated from the deposited mass and the thickness of the electrodes. It is also worth noting that the electrodes show lower

porosity near the electrode/electrolyte interface due to the faster evaporation rate of the solvents at the beginning of the deposition. This leads to graded porous electrodes with greater porosity on the cathode surface, which ensures efficient oxygen transport towards the reaction sites near the electrolyte/electrode interface (Fig 2a).

The most remarkable difference between the electrodes is the average grain size, which decreases after the CGO addition (Fig. 2b and 2c). The blank 100LSCF shows an average grain size of 80 nm after sintering at 800 ºC for 2 h. In the composite electrodes, no morphological differences between the CGO and LSCF particles are observed and their atomic numbers are not sufficiently different to distinguish both materials by backscattering SEM. The average particle size and grain size distribution of 50LSCF is smaller compared to 100LSCF, about 30 nm (Fig. 2c). This fact is explained by the presence of CGO as secondary phase, which limits the cation diffusion and the growth rate of LSCF particles, in accordance with previous studies [26,27,38].

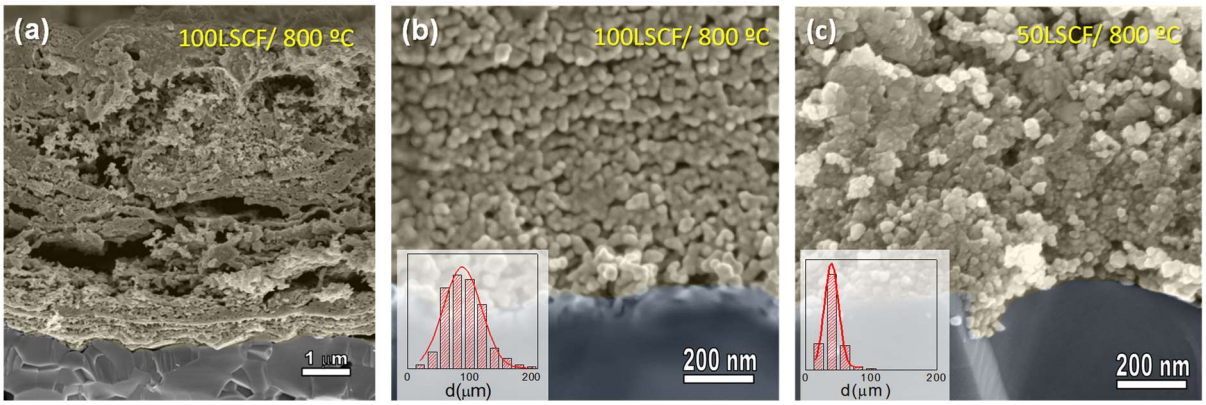

Fig. 2. SEM image of (a) - (b) 100LSCF at different magnifications and (c) 50LSCF calcined at 800 ºC for 2 h. The inset figures of (b) and (c) show the grain size distribution.

HAADF-STEM image and EDS elemental mapping reveal that CGO and LSCF particles are well distinguished and homogenously distributed, ensuring percolation of both phases and therefore increased TBP sites for the ORR (Fig. 3a). The increase of temperature at 1000 ºC results in a significant grain growth from 30 nm at 800 ºC to 50 nm at 1000 ºC as well as a drastic reduction of the porosity (Fig. 3b). This results in oxygen diffusion limitations, and therefore, the application of these electrodes was restricted at temperatures below 800 ºC.

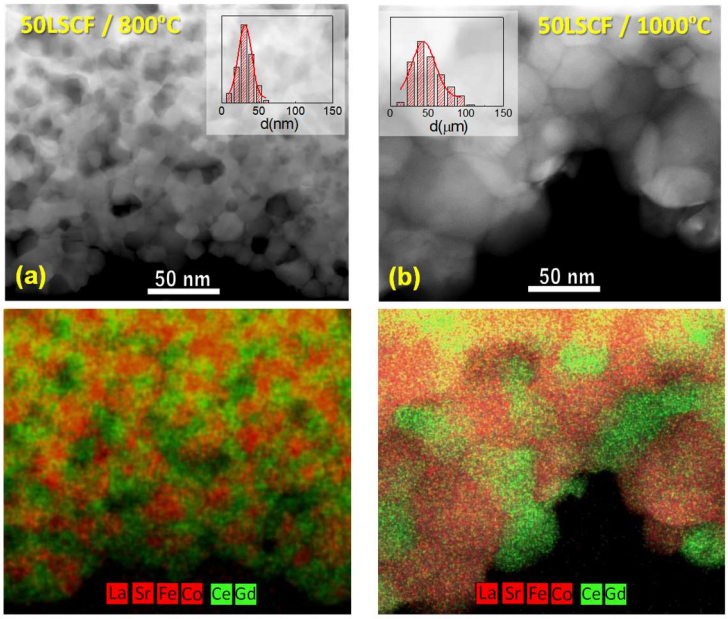

Fig. 3. HAADF-STEM image and EDS mapping of 50LSCF calcined at (a) 800 ºC and (b) 1000 ºC for 2 h. The inset figures show the grain size distribution.

3.3. Polarization resistance in symmetrical cells

The impedance spectra of the different LSCF-CGO/CGO/LSCF-CGO symmetrical cells, acquired under open circuit voltage at 600 ºC in air, are shown in Fig. 4. The electrode polarization is composed of two different contributions, which are simulated by using two serial (*RQ*) elements in series, where *R* is a resistance and *Q* a constant phase element (inset Fig. 4). The subscripts MF and LF denote the medium and low frequency responses, respectively. A serial resistance R_s and an inductance *L* are included to take into consideration the ohmic resistance of the electrolyte and the inductive effects of the setup, respectively. It is clear from Fig. 4 that the LSCF-CGO nanocomposites exhibit somewhat lower polarization resistance when compared to the blank 100LSCF. The lowest values of polarization resistance are found for the composite cathodes, containing between 50 and 60 wt.% of LSCF, in accordance with previous studies [22-24].

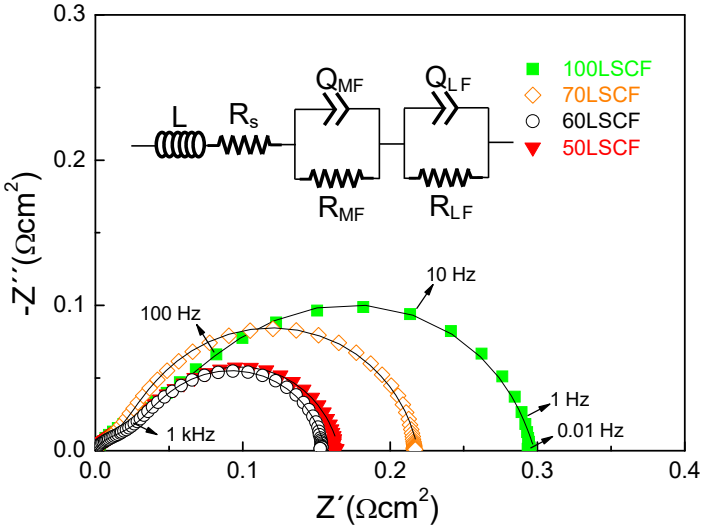

Fig. 4. Impedance spectra of the different LSCF-CGO composite cathodes in air at 600 ºC under open circuit voltage.

The different parameters, obtained from the equivalent circuit fitting, were used to determine the relaxation frequency f and capacitance values C, according to the following equations:

$$f = (2\pi RC)^{-1} \quad \text{(Eq. 1)}$$

$$C = R^{(1-n)/n} \cdot Q^{1/n} \quad \text{(Eq. 2)}$$

The variation of these magnitudes as a function of the temperature for 100LSCF and 50LSCF samples is shown in Fig. 5. The relaxation frequencies follow a typical Arrhenius behavior with the temperature. Despite the frequencies appear at somewhat higher values for the nanocomposite cathodes, the processes involved in the ORR for both samples seem to be similar (Fig. 5a).

Regarding the values of capacitance, these are clearly larger for 50LSCF than 100LSCF and this may be explained by the smaller particle size and larger contact area between CGO and LSCF particles (Fig. 5b). A similar behavior has also been observed for different nanostructured cathodes and attributed to their higher TPB length [30,39]. The LF response, typically associated with the dissociation adsorption of oxygen molecules, exhibits average capacitances of 15 and 70 mFcm^{-2} for 100LSCF and 50LSCF, respectively [40,41]. In contrast, the MF process has lower capacitance with respect to LF, i.e. 3 and 9 mFcm^{-2} for 100LSCF and 50LSCF, respectively, which is consistent with a charge transfer process [42,43].

The variation of the resistance contributions is plotted in Fig. 5c. For both samples, the resistance associated with the LF process is the dominant contribution, indicating that oxygen dissociation adsorption is the main rate limiting step to ORR. The activation energy of LF is also higher than that of MF, in accordance with the literature data, since the oxygen dissociative adsorption usually requires more energy to be activated than electron transfer [44]. The activation energy for MF is similar for both samples, about 1.08 eV. In contrast, the LF process exhibits lower activation energy for 50LSCF, 1.34 eV, than for 100 LSCF, 1.43 eV, indicating that the oxygen dissociation in the nanocomposite cathode is easier as the TPB sites increases with the CGO-addition.

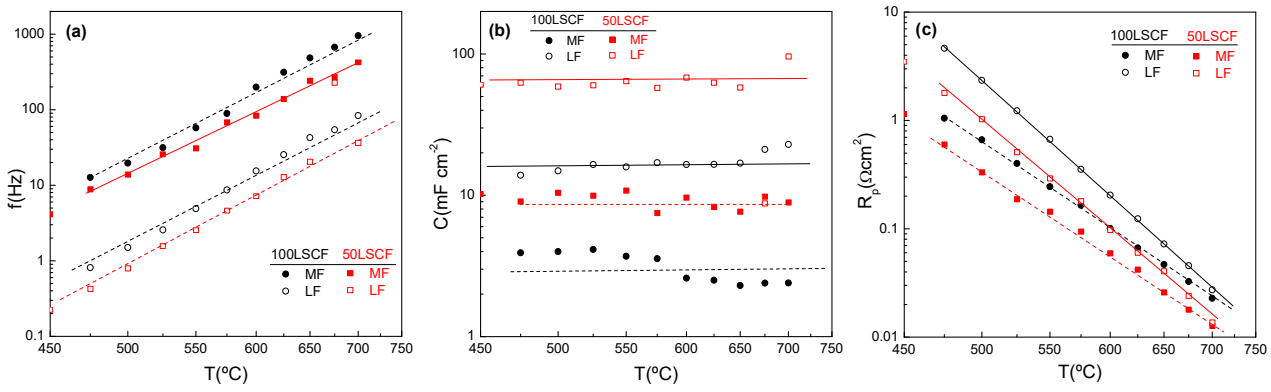

Fig. 5. Variation with the temperature of (a) the relaxation frequencies, (b) capacitances and (c) polarization resistances of the MF and LF contributions to the overall polarization for 100LSCF and 50LSCF cathodes.

Fig. 6 compares the variation of the overall polarization resistance with the temperature for the different electrodes. The data for a traditional composite cathode, 60LSCF, deposited by screen-printing at 1000 ºC for 1 h, are also included for the sake of comparison. As can be observed, the nanocomposite cathodes exhibit a polarization resistance one order of magnitude inferior to the traditional cathode. It is also

important to comment that all nanostructured electrodes exhibit similar polarization resistance, and especially in the high temperature range, e.g. 0.046 Ωcm^2 for 100LSCF and 0.032 Ωcm^2 for 50LSCF at 700 ºC. The differences are more important in the low temperature range, i.e. 16.4 Ωcm^2 for 50LSCF and 43.6 Ωcm^2 for 100LSCF at 400 ºC. Thus, the increase of TPB length by using LSCF-CGO nanocomposite cathodes has not drastic benefits in term of efficiency when compared to the blank cathode. The main advantage of CGO addition is the grain growth suppression, resulting in smaller particles with better microstructural stability at high annealing temperatures.

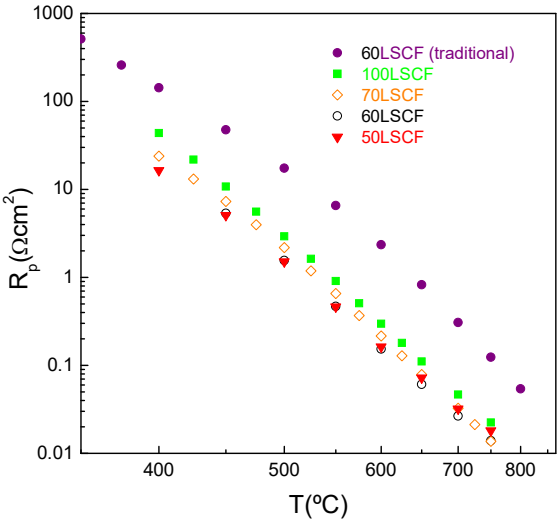

Fig. 6. Temperature dependence of the overall polarization resistance for the different LSCF-CGO nanocomposite cathodes. The data of a traditional 60LSCF cathode prepared by screen-printing method is also included for the sake of comparison.

3.4. Single cell performance

In order to test the performance of the nanocomposite cathodes in real SOFC conditions, NiO-CGO/CGO/60LSCF anode supported cells were prepared. Fig. 7 compares the current-voltage and power density curves of two cells with traditional and nanocomposite cathodes, using humidified hydrogen as fuel and static air as oxidant. It is worth noting that the anode supported cells were fabricated in a same batch to minimize performance variations associated with the anode and the electrolyte. Thus, the different performance of the cells is mainly attributed to the different cathode used.

The open circuit voltage (OCV) increases as the temperature decreases from 0.82 V at 650 ºC to 0.96 V at 500 ºC due to the n-type electronic conductivity of the CGO electrolyte under reducing atmosphere. These values are comparable to those previous reported, confirming excellent gas-tight sealing of the cell [47].

The cell with traditional cathode generates maximum power densities of 0.56 and 0.10 Wcm^{-2} at 650 and 500 ºC, respectively. In comparison, the cell with the nanocomposite cathode achieves improved power densities of 0.9 and 0.29 Wcm^{-2} at 650 and 500 ºC, respectively. Thus, the performance of this cell increases in a factor of 1.6 and 2.9 in the high and low temperature range, respectively. Note that the performance improvement is more important at low temperature, in accordance to the lowest values of polarization resistance obtained in symmetrical cells.

A short stability test of the cell was performed at 600 ºC during 72 h of operation. The power density increased slightly during the first hours and then remained almost constant over time (Fig. 7c), confirming negligible degradation of the cell.

Fig. 7d shows a cross-sectional image of the cell after the electrochemical characterization, the electrolyte is dense and has a thickness of about 20 µm and both cathode and anode present good porosity and adherence with the electrolyte. In addition, no appreciable microstructural coarsening of the cathode is observed with respect to the as-prepared material due to the low operating temperature used.

In summary, nanocomposite cathodes exhibit improved electrocatalytic properties for ORR compared to traditional electrodes prepared by screen-printing method. On the other hand, LSCF cathodes usually suffer performance degradation, caused by surface composition changes after long-term annealing at high temperature, i.e. superficial Sr-enrichment [45-47]. However, in these nanocomposite cathodes, the high contact between LSCF and CGO particles reduces the surface of LSCF exposed to air, and consequently, they would be less susceptible to surface carbonation. Thus, the long term stability in CO_2 containing atmospheres needs to be further investigated.

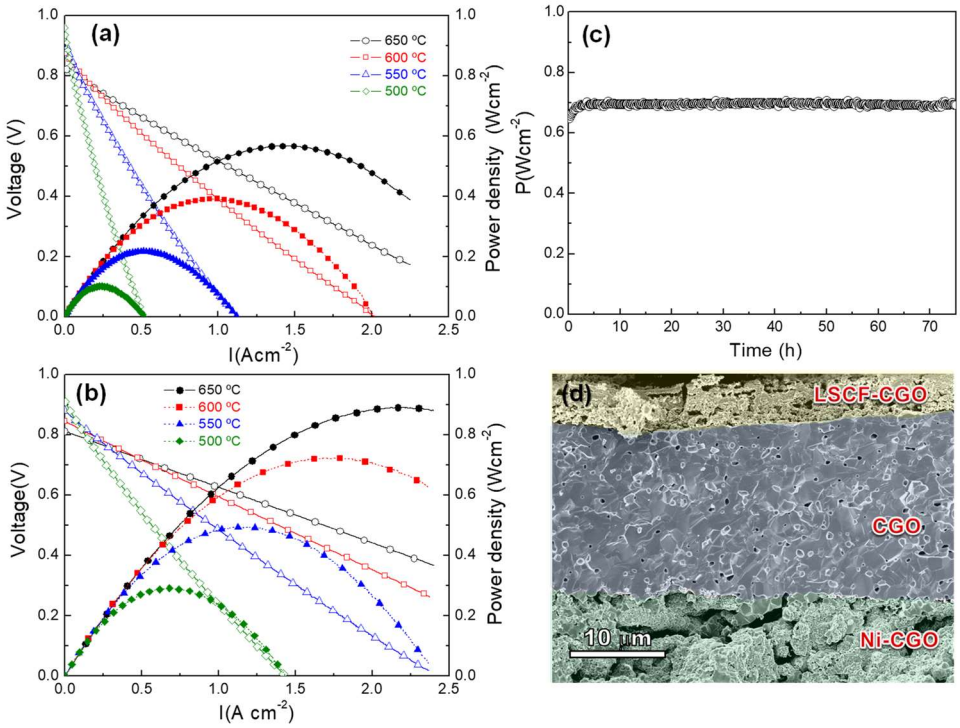

Fig. 7. Voltage and power density curves of NiO-CGO/CGO/60LSCF cells with (a) a traditional and (b) a nanocomposite cathode. (c) Variation of the power density for the cell with nanocomposite cathode over time at 600 ºC; (d) SEM cross-sectional image of the cell after the electrochemical test.

CONCLUSIONS

Nanocomposite cathodes of LSCF-CGO with different LSCF content from 50 to 100 wt.% were prepared by using a single spray-pyrolysis deposition method. A precursor solution containing all cations in stoichiometric amounts was used. In this way, LSCF and CGO are prepared simultaneously, reducing drastically the preparation time, which is an important improvement for industrial applications. No secondary phases were detected between 800 and 1000 ºC despite the co-synthesis of LSCF and CGO.

The CGO-addition partially supresses the grain growth of the nanocomposite cathodes, rendering lower particle size with respect to the blank cathode, i.e. 30 nm for 50LSCF and 80 nm for 100LSCF. The reduction of the grain size is the main reason for the polarization resistance improvement. This takes values at 600ºC of 0.30 and 0.15 Ωcm^2 for 100LSCF and 50 LSCF, respectively.

A single cell with 50LSCF nanocomposite cathode generated an improved power density of 0.90 Wcm^{-2} at 650 ºC, compared 0.56 Wcm^{-2} for a traditional cathode. Stability test over time at 600 ºC showed a negligible degradation of the cell.

.

ACKNOWLEDGEMENTS

This work has been supported by EC2014-53906-R and MAT2013-41836-R research grants (Spain). J.M. Porras-Vázquez thanks the University of Málaga for the funding. L. dos Santos-Gómez thanks to the Spanish Ministry of Education, Culture and Sports for her FPU grant.

REFERENCES

[1] D.J.L. Brett, A. Atkinson, N.P. Brandon, S.J. Skinner, Intermediate temperature solid oxide fuel cells, Chem. Soc. Rev. 37 (8) (2008) 1568-1578.

[2] A.B. Stambouli, E. Traversa, Solid oxide fuel cells (SOFCs): A review of an environmentally clean and efficient source of energy, Renew. Sustainable Energy Rev. 6 (5) (2002) 433-455.

[3] R.M. Ormerod, Solid oxide fuel cells, Chem. Soc. Rev. 32 (1) (2003) 17-28.

[4] Y. Zhang, R. Knibbe, J. Sunarso, Y. Zhong, W. Zhou, Z. Shao, Z. Zhu, Recent Progress on Advanced Materials for Solid-Oxide Fuel Cells Operating Below 500 °C, Adv. Mater. DOI: 10.1002/adma.201700132.

[5] S.P. Jiang, Development of lanthanum strontium manganite perovskite cathode materials of solid oxide fuel cells: A review, J. Mater. Sci. 43 (21) (2008) 6799-6833.

[6] S.B. Adler, Factors Governing Oxygen Reduction in Solid Oxide Fuel Cell Cathodes, Chem. Soc. Rev. 104 (2004) 4791-4843.

[7] C. Sun, R. Hui, J. Roller, Cathode materials for solid oxide fuel cells: A review, J. Solid State Electrochem. 14 (2010) 1125-1144.

[8] Z. Gao, L.V. Mogni, E.C. Miller, J.G. Railsback, S.A. Barnett, A perspective on low-temperature solid oxide fuel cells, Energy Environ. Sci. 9 (2016) 1602-1644.

[9] C.M. Chanquía, L. Mogni, H.E. Troiani, A. Caneiro, Highly active $La_{0.4}Sr_{0.6}Co_{0.8}Fe_{0.2}O_{3-\delta}$ nanocatalyst for oxygen reduction in intermediate temperature-solid oxide fuel cells, J. Power Sources 270 (2014) 457-467.

[10] C.H. Hua, C.C. Chou, Preparation of nanoscale composite LSCF/GDC cathode materials by microwave sintering for intermediate-temperature SOFC applications, Ceram. Int. 41 (2015) s708-s712.

[11] E. Zhao, C. Ma, W. Yang, Y. Xiong, J. Li, C. Sun, Electrospinning $La_{0.8}Sr_{0.2}Co_{0.2}Fe_{0.8}O_{3-\delta}$ tubes impregnated with $Ce_{0.8}Gd_{0.2}O_{1.9}$ nanoparticles for an intermediate temperature solid oxide fuel cell cathode, Int. J. Hydrogen Energy 38 (16) (2013) 6821-6829.

[12] A. Chrzan, J. Karczewski, M. Gazda, D. Szymczewska, P. Jasinski, $La_{0.6}Sr_{0.4}Co_{0.2}Fe_{0.8}O_{3-\delta}$ oxygen electrodes for solid oxide cells prepared by polymer precursor and nitrates solution infiltration into gadolinium doped ceria backbone, J. Eur. Ceram. Soc. 37 (11) (2017) 3559-3564.

[13] D. Beckel, U.P. Muecke, T. Gyger, G. Florey, A. Infortuna, L.J. Gauckler, Electrochemical performance of LSCF based thin film cathodes prepared by spray pyrolysis, Solid State Ionics 178 (2007) 407-415.

[14] P.L.B. Silva, R.P. Vieira, C.M. Halmenschlager, F.F. Oliveira, C.P. Bergmann, Low temperature synthesis by spray pyrolysis of $La_{0.9}Sr_{0.1}Co_{0.2}Fe_{0.8}O_3$ thin films using ethanol and water as a solvent and their microstructural characterization, Ceram. Int. 41 (10) (2015) 13304-13309.

[15] D. Marinha, C. Rossignol, E. Djurado, Influence of electrospraying parameters on the microstructure of $La_{0.6}Sr_{0.4}Co_{0.2}F_{0.8}O_{3-\delta}$ films for SOFCs, J. Solid State Chem. 182 (7) (2009) 1742-1748.

[16] D. Marinha, L. Dessemond, J.S. Cronin, J.R. Wilson, S.A. Barnett, E. Djurado, Microstructural 3D reconstruction and performance evaluation of LSCF cathodes obtained by electrostatic spray deposition, Chem. Mater. 23 (24) (2011) 5340-5348.

[17] A.P. Jamale, S.U. Dubal, S.P. Patil, C.H. Bhosale, L.D. Jadhav, Influence of substrate temperature on structural, morphological and electrical properties of $La_{0.6}Sr_{0.4}Co_{0.2}Fe_{0.8}O_3$ thin films for IT-SOFCs, Appl. Surf. Sci. 286 (2013) 78-82.

[18] D. Marrero-López, R. Romero, F. Martín, J.R. Ramos-Barrado, Effect of the deposition temperature on the electrochemical properties of $La_{0.6}Sr_{0.4}Co_{0.8}Fe_{0.2}O_{3-\delta}$ cathode prepared by conventional spray-pyrolysis, J. Power Sources 255 (2014) 308-317.

[19] A. Esquirol, J. Kilner, N. Brandon, Oxygen transport in $La_{0.6}Sr_{0.4}Co_{0.2}Fe_{0.8}O_{3-\delta}/Ce_{0.8}Ge_{0.2}O_{2-x}$ composite cathode for IT-SOFCs, Solid State Ionics 175 (2004) 63-67.

[20] J. Sar, L. Dessemond, E. Djurado, Electrochemical properties of graded and homogeneous $Ce_{0.9}Gd_{0.1}O_{2-\delta}$-$La_{0.6}Sr_{0.4}Co_{0.2}Fe_{0.8}O_{3-\delta}$ composite electrodes for intermediate-temperature solid oxide fuel cells, Int. J. Hydrogen Energy 41 (2016) 17037-17043.

[21] M.R. Cesario, D.A. Macedo, A.E. Martinelli, R.M. Nascimento, B.S. Barros, D.M.A. Melo, Synthesis, structure and electrochemical performance of cobaltite-based composite cathodes for IT-SOFC, Cryst. Res. Technol. 47 (2012) 723-730.

[22] Y. Leng, S.H. Chan, Q. Liu, Development of LSCF–GDC composite cathodes for low-temperature solid oxide fuel cells with thin film GDC electrolyte, Int. J. Hydrogen Energy 33 (2008) 3808-3817.

[23] V. Dusastre, J.A. Kilner, Optimisation of composite cathodes for intermediate temperature SOFC applications, Solid State Ionics 126 (1999) 163-174.

[24] E.P. Murray, M.J. Sever, S.A. Barnett, Electrochemical performance of $(La,Sr)(Co,Fe)O_3$-$(Ce,Gd)O_3$ composite cathodes, Solid State Ionics 148 (2002) 27-34.

[25] W.G. Wang, M. Mogensen, High-performance lanthanum-ferrite-based cathode for SOFC, Solid State Ionics 176 (2005) 457-462.

[26] B.F. Angoua, P.R. Cantwell, E.A. Stach, E.B. Slamovich, Crystallization and electrochemical performance of $La_{0.6}Sr_{0.4}Co_{0.2}Fe_{0.8}O_{3-\delta}$-$Ce_{0.8}Gd_{0.2}O_{1.9}$ thin film cathodes processed by single solution spray pyrolysis, Solid State Ionics 203 (1) (2011) 62-68.

[27] B.F. Angoua, E.B. Slamovich, Single solution spray pyrolysis of $La_{0.6}Sr_{0.4}Co_{0.2}Fe_{0.8}O_{3-\delta}$–$Ce_{0.8}Gd_{0.2}O_{1.9}$ (LSCF–CGO) thin film cathodes, Solid State Ionics 212 (2012) 10-17.

[28] Ö. Çelikbilek, E. Siebert, D. Jauffrès, C.L. Martin, E. Djurado, Influence of sintering temperature on morphology and electrochemical performance of LSCF/GDC composite films as efficient cathode for SOFC, Electrochim. Acta 246 (2017) 1248-1258.

[29] J. Sar, O. Celikbilek, J. Villanova, L. Dessemond, C.L. Martin, E. Djurado, Three dimensional analysis of $Ce_{0.9}Gd_{0.1}O_{1.95}$–$La_{0.6}Sr_{0.4}Co_{0.2}Fe_{0.8}O_{3-\delta}$ oxygen electrode for solid oxide cells, J. Eur. Ceram. Soc. 35 (16) (2015) 4497-4505.

[30] L. dos Santos-Gómez, E.R. Losilla, F. Martín, J.R. Ramos-Barrado, D. Marrero- López, Novel Microstructural Strategies To Enhance the Electrochemical Performance of $La_{0.8}Sr_{0.2}MnO_{3-\delta}$ Cathodes, ACS Appl. Mater. Inter. 7 (2015) 7197-7205.

[31] L. dos Santos-Gómez, J.M. Porras-Vázquez, F. Martín, J.R. Ramos-Barrado, E.R. Losilla, D. Marrero-López, An easy and innovative method based on spray-pyrolysis deposition to obtain high efficiency cathodes for Solid Oxide Fuel Cells, J. Power Sources 319 (2016) 48-55.

[32] X'Pert HighScore Plus, version 3.0e, PANalytical BV. Amelo, The Netherlands, 2012.

[33] A.C. Larson, R.B. von Dreele, GSAS Program, Los Alamos National Lab, 1994. Rep. No. LA-UR-86748.

[34] D. Johnson, ZView: Asoftware Program for IES Analysis, Version 2.8, Scribner Associates, Inc., Southern Pines, NC, 2002.

[35] L. dos Santos-Gomez, J.M. Porras-Vazquez, E.R. Losilla, D. Marrero-López, Improving the efficiency of layered perovskite cathodes by microstructural optimization, J. Mater. Chem. A 5 (2017) 7896-7904.

[36] Inorganic Crystal Structure Database, ICSD, 2017, pp. v2014-01.

[37] D. Pérez-Coll, D. Marrero-López, P. Núñez, S. Piñol, J.R. Frade, Grain boundary conductivity of $Ce_{0.8}Ln_{0.2}O_{2-\delta}$ ceramics (Ln=Y, La, Gd, Sm) with and without Co-doping, Electrochim. Acta 51 (28) (2006) 6463-6469.

[38] H. Shimada, T. Yamaguchi, H. Sumi, K. Nomura, Y. Yamaguchi, Y. Fujishiro, Extremely fine structured cathode for solid oxide fuel cells using Sr-doped $LaMnO_3$ and Y_2O_3-stabilized ZrO_2 nano-composite powder synthesized by spray pyrolysis, J. Power Sources 341 (2017) 280-284.

[39] L. Wu, Z. Jiang, S. Wang, C. Xia, $(La,Sr)MnO_3$–$(Y,Bi)_2O_3$ composite cathodes for intermediate-temperature solid oxide fuel cells, Int. J. Hydrogen Energy 38 (5) (2013) 2398-2406.

[40] L. Nie, M. Liu, Y. Zhang, M. Liu, $La_{0.6}Sr_{0.4}Co_{0.2}Fe_{0.8}O_{3-\delta}$ cathodes infiltrated with samarium-doped cerium oxide for solid oxide fuel cells, J. Power Sources 195 (2010) 4704-4708.

[41] X.Y. Xu, Z.Y. Jiang, X. Fan, C.R. Xia, LSM-SDC electrodes fabricated with an ion-impregnating process for SOFCs with doped ceria electrolytes, Solid State Ionics 177 (2006) 2113-2117.

[42] D. Waller, J.A. Lane, J.A. Kilner, B.C.H. Steele, The effect of thermal treatment on the resistance of LSCF electrodes on gadolinia doped ceria electrolytes, Solid State Ionics 86 (1996) 767-772.

[43] F. Bidrawn, R. Küngas, J.M. Vohs, R.J. Gorte, Modeling Impedance Response of SOFC Cathodes Prepared by Infiltration, J. Electrochem. Soc. 158 (5) (2011) B514-B525.

[44] Y. Gong, R.L. Patel, X. Liang, D. Palacio, X. Song, J.B. Goodenough, K. Huang, Atomic Layer Deposition Functionalized Composite SOFC Cathode $La_{0.6}Sr_{0.4}Fe_{0.8}Co_{0.2}O_{3-\delta}$ -$Gd_{0.2}Ce_{0.8}O_{1.9}$: Enhanced Long-Term Stability, Chem. Mater. 25 (2013) 4224-4231.

[45] L. Agun, H.A. Rahman, S. Ahmad, A. Muchtar, Durability and stability of LSCF composite cathode for intermediate-low temperature of solid oxide fuel cell (IT-LT SOFC): Short review, Adv. Mat. Res. 893 (2014) 732-737.

[46] H. Wang, K.J. Yakal-Kremski, T. Yeh, G.M. Rupp, A. Limbeck, J. Fleig, S.A. Barnet, Mechanisms of Performance Degradation of $(La,Sr)(Co,Fe)O_{3-\delta}$ Solid Oxide Fuel Cell Cathodes, J. Electrochem. Soc. 163 (2016) F581-F585.

[47] L. dos Santos-Gómez, J.M. Porras-Vázquez, E.R. Losilla, F. Martín, J.R. Ramos-Barrado, D. Marrero-López, Stability and performance of $La_{0.6}Sr_{0.4}Co_{0.2}Fe_{0.8}O_{3-\delta}$ nanostructured cathodes with $Ce_{0.8}Gd_{0.2}O_{1.9}$ surface coating, J. Power Sources 347 (2017) 178-185.